Bond-Breaking Efficiency of High-Energy Ions in Ultrathin Polymer Films

R. Thomaz,[1,*] P. Louette,[2] G. Hoff,[3] S. Müller,[1] J. J. Pireaux,[2] C. Trautmann,[4,5] and R. M. Papaléo[1]
[1]Interdisciplinary Center of Nanoscience and Micro-Nanotechnology, School of Sciences, Pontifical Catholic University of Rio Grande do Sul, Avenida Ipiranga 6681, 90619-900 Porto Alegre, Brazil
[2]Université de Namur, Rue de Bruxelles 61, 5000 Namur, Belgium
[3]Università di Cagliari and IFN Sex. Di Cagliari- Dipartimento di Fisica, I-09042 Monserrato (CA), Italy
[4]GSI Helmholtzzentrum für Schwerionenforschung, Planckstrasse 1, 64291 Darmstadt, Germany
[5]Technische Universität Darmstadt, Alarich-Weiss-Strasse 2, 64287 Darmstadt, Germany

(Received 30 January 2018; published 6 August 2018)

Thin films of poly(methyl methacrylate) and poly(vinyl chloride) of different thickness are used to investigate the effect of spatial confinement on the efficiency of bond breaking induced by 2 MeV H^+ and 2.1 GeV Bi ions. Effective cross sections for oxygen and chlorine loss are extracted for films down to a thickness of about 5 nm and are compared to theoretical estimations based on radial energy density profiles simulated with GEANT-DNA. The cross sections are to a large extent thickness independent, indicating that bond breaking is dominated by short-range processes. This is in contrast to the strongly reduced efficiencies found recently for cratering induced by high-energy ions in similar ultrathin polymer films [Phys. Rev. Lett. **114**, 118302 (2015)].

DOI: 10.1103/PhysRevLett.121.066101

Polymers and other organic materials, including biological tissues, are very sensitive to ionizing radiation and degrade easily at relatively small doses [1,2]. This may result in a loss of functionality and dramatic changes in their original properties or, in the case of living matter, in severe biological effects. Among high-energy radiations, heavy ions have the highest levels of local energy transfer and hence very large damage efficiencies, usually estimated by measuring cross sections for the different processes involved [3–7]. Such an ability of energetic ions to severely transform the chemical structure of organic matter has been explored in a wide range of applications from the engineering of new materials and nanostructures [8,9] to cancer treatment [10] and has important implications to space exploration [11,12] and astrophysical issues [3].

Here we concentrate on fast ions for which the energy loss is dominated by electronic excitation. In this regime, bond breaking and the production of new chemical species is mainly controlled by the distribution of energy deposited by the emitted secondary electrons [12–16]. For very thin films, when the thickness is smaller than the extent of the secondary electron cascades, a fraction of such electrons may escape the material, reducing the local dose. Therefore, the damage yield may also decrease, a critical issue already noted in radiation effects at small target volumes such as cells or DNA [17,18]. Indeed, we have recently shown that cratering induced by individual ion impacts is substantially weakened in polymer ultrathin films because of the suppression of long-range cooperative effects that contribute to the total energy and momentum density deposited at the near surface [19]. Here, we address the fundamental problem of bond-breaking efficiency—a crucial aspect underlying the overall response of organic materials to radiation—under the spatial confinement conditions of ultrathin films. Contrary to cratering efficiency, we found bond-breaking cross sections in poly(methyl methacrylate) (PMMA) and poly(vinyl chloride) (PVC) thin films to be insensitive to thickness reductions, even in layers as thin as 5 nm.

Solutions at different concentrations of nearly monodisperse PMMA and PVC were spun onto silicon substrates to obtain films of initial thicknesses h varying from ~2 up to 290 nm. The samples were bombarded at normal incidence by 2.1 GeV Bi ions with charge state distribution around equilibrium at the UNILAC accelerator of GSI (Darmstadt, Germany) or with 2 MeV H^+ ions at the 3 MV Tandetron at Porto Alegre, Brazil. The fluence range was 10^{10} to 7×10^{11} Bi/cm^2 or 10^{14} to 2.8×10^{15} H^+/cm^2. For both projectiles, the energy deposition in the films is dominated by electronic processes, and the ions are stopped deep in the Si substrate. X-ray photoelectron spectroscopy (XPS) was performed on a ThermoFisher K-α spectrometer. Details of experimental procedures are given in Supplemental Material [20].

Figure 1 shows the C1s XPS spectra of PVC and PMMA films of different thicknesses before and after bombardment with 2 MeV H^+ and 2.1 GeV ions. The C1s PVC spectra [21,22] were deconvoluted to four peaks [Fig. S1(a) [20]], C_1—C (~286 eV) and C_2—Cl (~287 eV), and two additional components due to unsaturated carbon bonds (C_3 at 285 eV) and oxidized carbon groups (C_4 at 288–289 eV). The C1s PMMA spectra [23,24] were fitted with four peaks

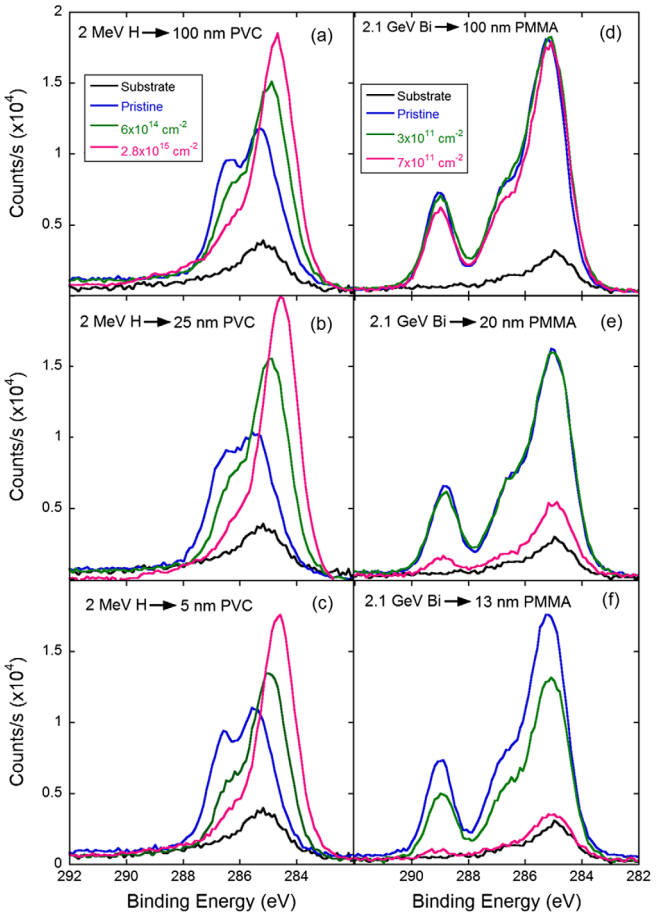

FIG. 1. C1s XPS spectra irradiated thin films of PVC (a)–(c) and PMMA (d)–(f). For PVC, spectra from (a) 100, (b) 25, and (c) 5 nm films irradiated with 2 MeV H^+ are shown. For PMMA, spectra from (d) 100, (e) 20, and (f) 13 nm films irradiated with 2.1 GeV Bi ions are depicted. The black lines are the spectra of Si substrates irradiated either with 2.5×10^{15} H/cm^2 or 7×10^{11} Bi/cm^2.

assigned to the aliphatic hydrocarbon (C_1—C and C_1—H at 285.0 eV), the ester oxygen-induced β-shifted carbon (C_2—C = O, 285.7 eV), the methyl ester (C_3—O, 286.8 eV), and the carboxyl carbon (C_4 = O, 288.9 eV).

Bond breaking induced by irradiation of PMMA has already been extensively studied, and general trends for thick films seen here are in agreement with previous results [5,25,26]. The main effect on PMMA is the loss of oxygen-rich moieties from the side chain (Fig. 1). For PVC, there is a marked change in the C bonding state due to strong dehydrochlorination (seen by the reduction in the C_2—Cl and Cl2p peaks) and to the formation of carbon double bonds (associated with an increase and energy shift of the C_3 peak).

Here our interest is to evaluate the bond-breaking efficiency of the energetic ions in films of different thicknesses. To this end, we measured the areas of the C—Cl (PVC) and C—O (PMMA) XPS peaks as a function of irradiation fluence ϕ. This requires a careful investigation of the changes in the sample conditions (thickness and porosity) and of the contribution of carbon grown during irradiation, especially when ultrathin layers are analyzed. The carbon contamination was estimated measuring the C1s peak intensities on highly irradiated Si substrates. The results (Fig. 1) are compatible with a layer of about 1 nm of carbon, with a low content of oxygenated species (additional data are given in Supplemental Material [20]). This gives an upper limit to the carbon contamination layer expected on the polymer films. For quantitative analysis, we considered only samples with a total carbon area 3 times larger than the peak of carbon contaminants on highly irradiated silicon. This limited the minimum analyzable initial thickness to 4 nm for 2 MeV H^+ irradiations. For the 2.1 GeV Bi beam, the pronounced thinning of the films [27] requires samples with a minimum initial thickness of 20 nm, if the quantification criterion is to be met for the full set of fluences.

The relative intensity I of the XPS signal was obtained in the case of PVC taking the ratio of the total chlorine to the total carbon peaks. For PMMA, the ratio of the C_3 or C_4 areas to the sum of the C_1 and C_2 peaks was used. Analyzing intensity ratios based on a reference element minimizes variations of the XPS signal due to changes in thickness induced by the irradiation. The values of I as a function of fluence ϕ and for different film thicknesses h are shown in Fig. 2. The solid lines are exponential fits to extract the cross sections σ for bond breaking:

$$I(\phi) = I_0 \exp(-\sigma\phi), \tag{1}$$

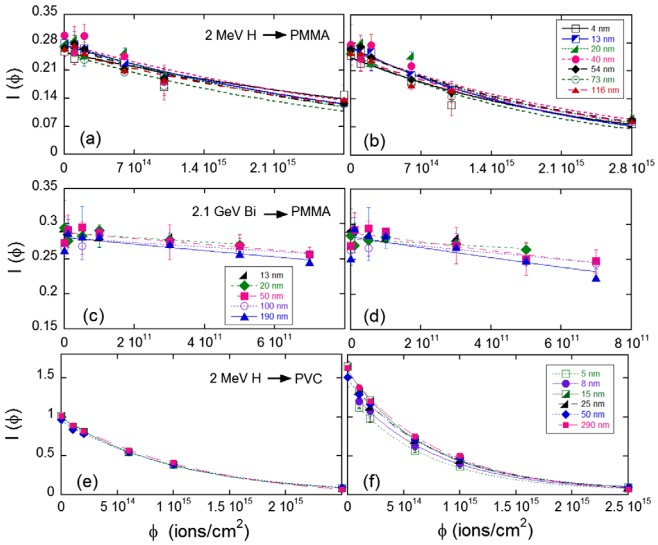

FIG. 2. Relative intensity of deconvoluted C1s XPS peaks as a function of fluence for various thicknesses. (a) C_3 (CH_3—O) and (b) C_4 (C = O) peaks of PMMA irradiated by 2 MeV H^+. (c) C_3 and (d) C_4 peaks of PMMA irradiated by 2.1 GeV ions. (e) Chlorine peak of PVC irradiated by 2 MeV H^+ using the ratios Cl:$(C_1 + C_3 + C_4)$ and (f) Cl:C_{total}.

where σ represents the effective area around the ion path where a given bond is destroyed [4] and is a measure of the radiolytic efficiency.

The signal intensity of samples of PVC and PMMA bombarded by 2 MeV H^+ could be well fitted by Eq. (1) (Fig. 2). The extracted damage cross sections for oxygen and chlorine loss are shown in Fig. 3. For the 2 MeV H^+ irradiations, no significant variations in σ are observed in the entire range of thicknesses. The σ values may change slightly, if different ways of estimating $I(\phi)$ are used, as shown in Fig. 3(a) for the PVC data, but not the dependence of σ on h. The data for the 2.1 GeV Bi irradiations were more difficult to analyze. The high dE/dx of these ions provokes substantial material loss due to sputtering, and the thinnest films are completely eroded (except for the adventitious carbon), before high levels of chemical damage are introduced in the samples. Therefore, the XPS data shown in Figs. 2(c) and 2(d) do not reach the typical exponential form needed for a precise fitting using Eq. (1). Cratering also induces porosity in the films [27], adding further uncertainties in the XPS analysis. As a result, the error bars of the extracted σ of carbon-oxygen bonds for the Bi beam shown in Fig. 3(c) are rather large. There is a trend of σ to decrease at $h = 20$ nm, but differences are within the uncertainties of the measurements.

The present finding of film thickness independence is very different from our previous results on crater and hillock formation in similar polymer films. Such radiation

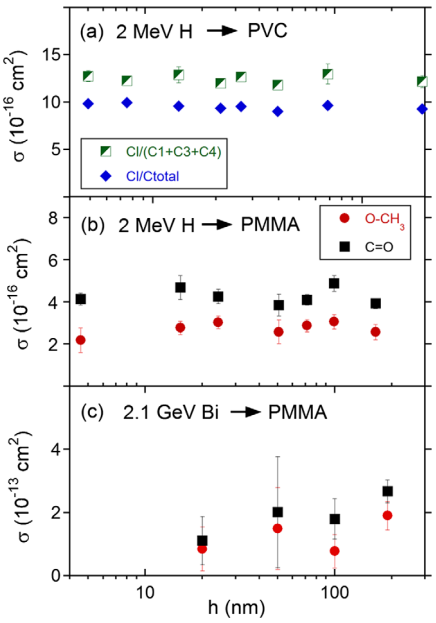

FIG. 3. Chemical damage cross sections σ of PVC and PMMA films of different thicknesses h. (a) Cross sections of chlorine loss (C—Cl bonds) in PVC irradiated by 2 MeV H^+ deduced from the ratio of the total chlorine to the total carbon peaks $Cl:C_{total}$ (blue) or from the ratio $Cl:(C_1 + C_3 + C_4)$ (green). Carbon-oxygen bonds from PMMA irradiated by (b) 2 MeV H^+ and (c) 2.1 GeV ions. The uncertainties given are fitting errors.

effects are substantially reduced for $h < 40$ nm, because they depend on the sum of excitations along the ion track length [19]. Here, on the contrary, bond breaking is dominated by local, short-range processes: Material excitation at deep layers is of no relevance for the near-surface chemistry seen by XPS. However, as noted previously, even the local deposited energy is expected to decrease in very thin layers. In order to estimate such changes and the impact on the damage cross sections, we performed Monte Carlo (MC) simulations using GEANT4-DNA (version 10.02 path 01), a code especially designed to model radiation processes at the nanoscale and widely used in radiobiology [28–31]. As interaction cross sections for protons and electrons are so far validated only for water and beams of Bi ions are not available, we run, as a first approximation, simulations in thin layers of water ($2 < h < 200$ nm, 1 g/cm^3) on a water substrate bombarded by 2 MeV H^+. A total of 10^5 incident ions were simulated in order to obtain the longitudinal and radial deposited energy distributions in the tracks. More details are given in Supplemental Material [20].

The simulated linear energy transfer $\Delta E(z)/\Delta z$ (the mean energy deposited in a slice of thickness Δz at a depth z inside the film), and the mean radial energy density $\epsilon(r,h) = \Delta E_{\text{shell}}/V_{\text{shell}}$ (where ΔE_{shell} is the average energy deposited in the volume V_{shell} of a thin cylindrical shell of radius r, thickness Δr, and length h) are shown in Fig. 4. $\Delta E(z)/\Delta z$ is strongly reduced at points close to the surface (up to ~50%) and reaches the typical values of bulk PMMA only when the thickness is close to the maximum range of the δ rays [Fig. 4(a)]. In addition, at a given radial distance r from the impact point, the radial energy density $\epsilon(r,h)$ is systematically smaller the thinner the film is [Fig. 4(b)]. This decrease is more pronounced at large r (e.g., at $r = 50$ nm, there is a reduction by a factor of ~10 between films of $h = 2$ and $h = 100$ nm).

The influence of $\epsilon(r,h)$ on the cross section for bond breaking $\sigma(h)$ can be evaluated, noting that in the cylindrical geometry of an ion track

$$\sigma(h) = 2\pi \int_0^{R_u} P(r,h) r dr, \tag{2}$$

where $P(r,h)$ is the probability of breaking a bond at a distance r and R_u is the maximum range of the secondary electrons. $P(r,h)$ is directly related to $\epsilon(r,h)$ and can be estimated in different ways. Here we tested two schemes: the approach derived from the hit model [4] and a standard activated process [7] described, respectively, by

$$P(r,h) = \{1 - \exp[-\epsilon(r,h)/\epsilon_0]\}^m, \tag{3a}$$

$$P(r,h) = \exp[-\epsilon_0'/\epsilon(r,h)], \tag{3b}$$

where ϵ_0 and ϵ_0' are critical energy densities for bond breaking and m is the number of hits necessary to damage

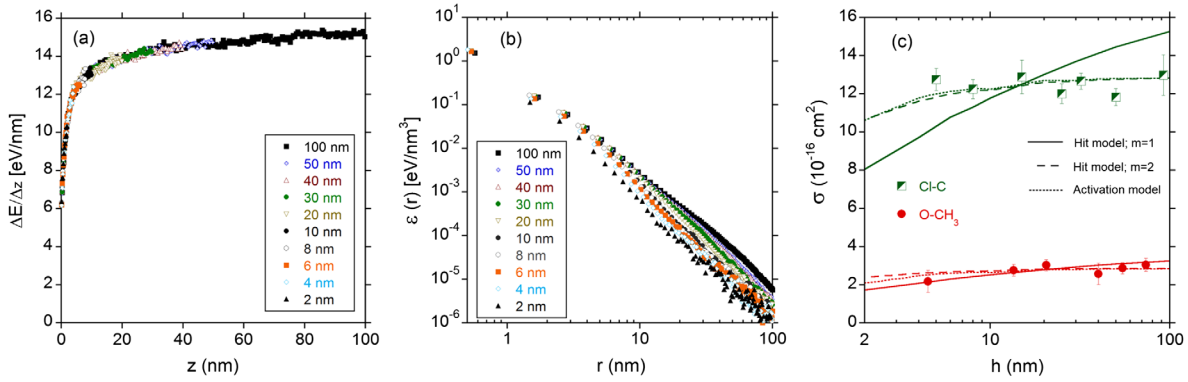

FIG. 4. Results from MC simulations of 2 MeV H^+ in water films. (a) Linear energy transfer $[\Delta E(z)/\Delta z]$ as a function of depth z; (b) deposited energy density as a function of radial distance r from the track center; (c) damage cross sections calculated from the simulated $\epsilon(r)$ curves of (b) using different laws of bond-breaking probability. Experimental cross sections for the polymer films are also shown for comparison. The ϵ_0 values for Cl loss are 73.6 (hit model, $m = 1$), 6.0 (hit model, $m = 2$), and 4.8 $\mathrm{eV/nm^3}$ (activation model), and for O—CH_3 bonds are 344.3 (hit, $m = 1$), 13.7 (hit, $m = 2$), and 7.6 $\mathrm{eV/nm^3}$ (activation).

the sensitive target. The simulated curves of $\epsilon(r, h)$ were used to estimate $P(r, h)$ and $\sigma(h)$ for the proton beam, having ϵ_0 as a free parameter. The curves of $P(r)$ as a function of the energy density for each model are presented in Fig. S6 [20]. The cross sections obtained using the two probability functions of Eqs. (3a) and (3b) are shown as lines in Fig. 4(c). Good agreement can be obtained between experimental and calculated cross sections, with a suitable choice of ϵ_0, ϵ_0', and m. The constraint applied to compare models was to force cross sections at $h = 15$ nm to be equal to the experimental values. This thickness was chosen because it corresponds roughly to the maximum XPS sampling depth in a polymer. The fitting parameters obtained under such condition are given in Fig. 4(c).

Overall, the calculated σ vary little with thickness (except for the one-hit model, when used to fit the PVC data). The weak dependence of σ on h stems from the fact that the variation of $\epsilon(r, h)$ with thickness is pronounced only at relatively large r [Fig. 4(b)], where $\epsilon(r, h)$ is already too small to contribute substantially to bond breaking. In the one-hit model ($m = 1$), $P(r)$ decreases much more slowly at small $\epsilon(r)$ than in the activation scheme (Fig. S6); hence, events at large r still make a significant contribution to σ, resulting in the stronger dependence of σ with h seen in Fig. 4(c). We also note that, in the simulations, electrons crossing the interface of the sensitive volume with the substrate still travel in the same material. In a real polymer-Si interface, electron backscattering may be larger and make energy suppression by spatial confinement even less evident, as the remarkable constancy of the experimentally measured σ suggests.

It is not surprising that for the 2 MeV H^+ beam very little differences in σ were observed in films down to a thickness of ~5 nm. Most of the bond breaking and Cl and O loss seen by XPS originates from low-energy (< 50 eV) secondary electrons with ranges below 5 nm. In addition, for the 2 MeV H^+ beam, only the energy deposition events close to the track core (which are least affected by thickness reductions) contribute significantly to σ. The rarer energy deposition events occurring at large r, which are clearly suppressed in thinner films, play a minimal role in the type of bond breaking probed here. They might, nevertheless, be important for other processes requiring lower activation energies. For heavier ions at larger velocities, thickness-dependent effects are expected to show up in thicker films, because regions far from the core [where the variation of $\epsilon(r)$ with h is stronger] can still make significant contributions to bond breaking. The results of the 2.1 GeV Bi ions irradiations [Fig. 3(c)] indicate this trend but are too "noisy" to allow a definitive answer. We note that effects of energy suppression at small length scales are also expected in the regime where ballistic damage dominates, because the damage is small at the start of the collision cascades and becomes significant only when the ions slow down deeper in a solid [32]. Nuclear stopping, however, plays a minimum role in our case.

In conclusion, confining a polymer in one of its spatial dimensions, as in ultrathin films, does not change significantly the efficiency of bond breaking induced by high-energy ions. This is evidenced both experimentally and in calculations based on simulated thickness-dependent radial energy density profiles calculated with GEANT4-DNA. In our experiments, radiolysis linked to heteroatom loss was probed. This involves relatively strong rearrangements of the chains and multiple bond breaking. Such processes occur mostly close to the ion path center, where changes in the deposited energy density with the thickness are small. Additional experiments targeting more sensitive, long-range probes for bond breaking (e.g., molecular weight distributions) are needed to test a spectrum of milder radiolytic processes, for which stronger spatial confinement effects are expected.

The brazilian agencies CNPq, CAPES, and FAPERGS are acknowledged for financial support.

*raquel.thomaz@pucrs.br

[1] A. Chapiro, *Radiation Chemistry of Polymeric Systems* (Interscience, Geneva, 1962), p. 728.

[2] D. Fink, *Fundamentals of Ion-Irradiated Polymers* (Springer, New York, 2004), p. 406.

[3] W. Portugal, S. Pilling, P. Boduch, H. Rothard, and D. P. P. Andrade, Mon. Not. R. Astron. Soc. **441**, 3209 (2014).

[4] R. Barillon, M. Fromm, R. Katz, and A. Chambaudet, Radiation Protection Dosimetry **99**, 359 (2002).

[5] M. Fragalà, G. Compagnini, A. Licciardello, and O. Puglisi, J. Polym Sci. B: Polym. Phys. **36**, 655 (1998).

[6] R. M. Papaleo, P. Demirev, J. Eriksson, P. Hakansson, B. U. R. Sundqvist, and R. E. Johnson, Phys. Rev. Lett. **77**, 667 (1996).

[7] R. M. Papaleo, A. Hallen, B. U. R. Sundqvist, L. Farenzena, R. P. Livi, M. A. deAraujo, and R. E. Johnson, Phys. Rev. B **53**, 2303 (1996).

[8] C. Trautmann, in *Ion Beams in Nanoscience and Technology* (Springer, New York, 2009), p. 457.

[9] J. A. van Kan, P. Malar, and Y. H. Wang, Appl. Surf. Sci. **310**, 100 (2014).

[10] J. S. Loeffler and M. Durante, Nat. Rev. Clin. Oncol. **10**, 411 (2013).

[11] V. K. Parihar, B. Allen, K. K. Tran, T. G. Macaraeg, E. M. Chu, S. Kwok, N. N. Chmielewski, B. M. Craver, J. E. Baulch, M. M. Acharya, F. A. Cucinotta, and C. L. Limoli, Sci. Adv. **1**, e1400256 (2015).

[12] M. Durante and F. A. Cucinotta, Nat. Rev. Cancer **8**, 465 (2008).

[13] A. Mozumder, Advan. Radiat. Chem. **1**, 1 (1969).

[14] R. Fleischer, P. Price, and R. Walker, *Nuclear Tracks in Solids: Principles and Applications* (University of California Press, Berkeley, 1975), p. 622.

[15] J. L. Magee and A. Chatterjee, in *Kinetics of Nonhomogeneous Processes: A Practical Introduction for Chemists, Biologists, Physicists, and Materials Scientists* (Springer, New York, 2009), p. 457.

[16] T. Elsasser, R. Cunrath, M. Kramer, and M. Scholz, New J. Phys. **10**, 075005 (2008).

[17] H. Nikjoo and D. T. Goodhead, Phys. Med. Biol. **36**, 229 (1991).

[18] F. A. Cucinotta, H. Nikjoo, and D. T. Goodhead, Radiat. Res. **153**, 459 (2000).

[19] R. M. Papaleo, R. Thomaz, L. I. Gutierres, V. M. de Menezes, D. Severin, C. Trautmann, D. Tramontina, E. M. Bringa, and P. L. Grande, Phys. Rev. Lett. **114**, 118302 (2015).

[20] See Supplemental Material at http://link.aps.org/supplemental/10.1103/PhysRevLett.121.066101 for technical details on the experimental analysis and GEANT4-DNA simulations.

[21] K. Hiraoka, Y. Iijima, and Y. Sakai, Surf. Interface Anal. **43**, 236 (2011).

[22] P. Louette, F. Bodino, and J.-J. Pireaux, Surf. Sci. Spectra **12**, 111 (2005).

[23] D. Briggs, *Surface Analysis of Polymers by XPS and Static SIMS* (Cambridge University Press, Cambridge, England, 1998).

[24] P. Louette, F. Bodino, and J. Pireaux, Surf. Sci. Spectra **12**, 69 (2005).

[25] U. H. Hossain, V. Lima, O. Baake, D. Severin, M. Bender, and W. Ensinger, Nucl. Instrum. Methods Phys. Res., Sect. B **326**, 135 (2014).

[26] D. Fink, L. Chadderton, F. Hosoi, H. Omichi, T. Sasuga, A. Schmoldt, L. Wang, R. Klett, and J. Hillenbrand, Nucl. Instrum. Methods Phys. Res., Sect. B **91**, 146 (1994).

[27] R. Thomaz, L. I. Gutierres, J. Morais, P. Louette, D. Severin, C. Trautmann, J. J. Pireaux, and R. M. Papaléo, Nucl. Instrum. Methods Phys. Res., Sect. B **365**, 578 (2015).

[28] S. Incerti, G. Baldacchino, M. Bernal, R. Capra, C. Champion, Z. Francis, P. Gueye, A. Mantero, B. Mascialino, P. Moretto, P. Nieminen, A. Rosenfeld, C. Villagrasa, and C. Zacharatou, Int. J. Model. Simul. Sci. Comput. **1**, 157 (2010).

[29] S. Incerti, M. Douglass, S. Penfold, S. Guatelli, and E. Bezak, Phys. Med. **32**, 1187 (2016).

[30] Geant4-DNA Collaboration, Geant4-DNA: Physics, http://geant4-dna.org.

[31] Geant4-Collaboration, Geant4 Cross Reference, http://www-geant4.kek.jp/lxr/source/.

[32] E. Zarkadoula, S. L. Daraszewicz, D. M. Duffy, M. A. Seaton, I. T. Todorov, K. Nordlund, M. T. Dove, and K. Trachenko, J. Phys. Condens. Matter **25**, 125402 (2013).